



Universiteit
Leiden
The Netherlands

Disentangling drought-responsive traits with focus on *Arabidopsis*

Thonglim, A.

Citation

Thonglim, A. (2023, November 9). *Disentangling drought-responsive traits with focus on Arabidopsis*. Retrieved from <https://hdl.handle.net/1887/3656528>

Version: Publisher's Version

License: [Licence agreement concerning inclusion of doctoral thesis in the Institutional Repository of the University of Leiden](#)

Downloaded from: <https://hdl.handle.net/1887/3656528>

Note: To cite this publication please use the final published version (if applicable).

Chapter 2

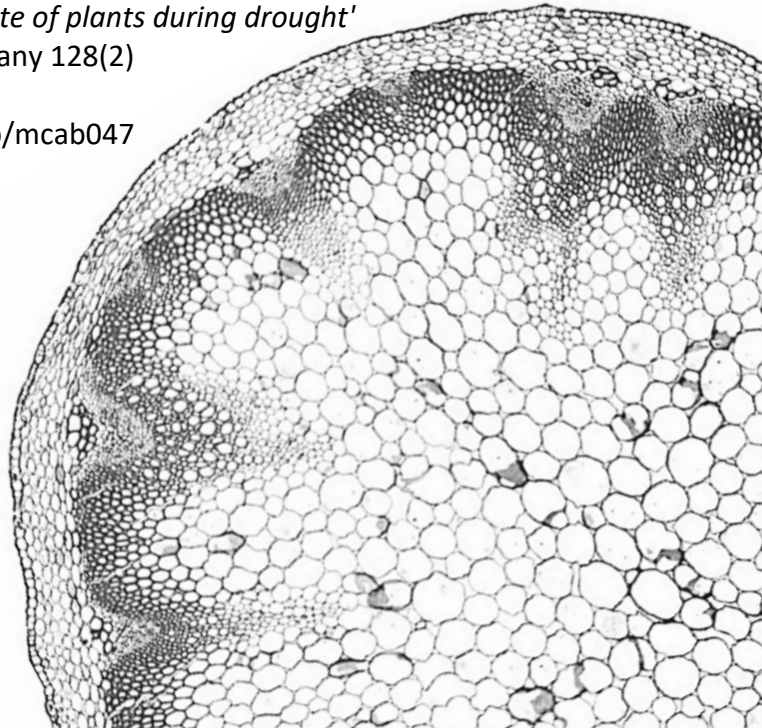
Intervessel pit membrane thickness best explains variation in embolism resistance amongst stems of *Arabidopsis thaliana* accessions

Ajaree Thonglim^{1*}, Sylvain Delzon², Maximilian Larter¹, Omid Karami³, Arezoo Rahimi³, Remko Offringa³, Joost J. B. Keurentjes⁴, Salma Balazadeh³, Erik Smets¹, and Frederic Lens^{1*}

Adapted from

Annals of Botany 128(2) (2021, first published online in 2020): 171-182.
<https://doi.org/10.1093/aob/mcaa196>

A commentary paper by Craig R. Brodersen, entitled '*By the narrowest of margins: nano-scale modification of pit membranes and the fate of plants during drought*' is published in *Annals of Botany* 128(2) (2021): iii-v.
<https://doi.org/10.1093/aob/mcab047>



¹ Naturalis Biodiversity Center, Functional Traits, PO Box 9517, 2300 RA Leiden, The Netherlands

² BIOGECO INRA, Université Bordeaux, 33615 Pessac, France

³ Plant Developmental Genetics, Institute of Biology Leiden, Leiden University, 2333 BE Leiden, the Netherlands

⁴ Laboratory of Genetics, Wageningen University, Droevendaalsesteeg 1, 6708 PB Wageningen, The Netherlands

*For correspondence. E-mail: ajaree.thonglim@naturalis.nl;
frederic.lens@naturalis.nl

Abstract

The ability to avoid drought-induced embolisms in the xylem is one of the essential traits for plants to survive periods of water shortage. Over the past three decades, hydraulic studies have been focusing on trees, which limits our ability to understand how herbs tolerate drought. Here, we investigate the embolism resistance in inflorescence stems of four *Arabidopsis thaliana* accessions that differ in growth form and drought response. We assess functional traits underlying the variation in embolism resistance amongst the accessions studied using detailed anatomical observations. The vulnerability to xylem embolism was obtained via vulnerability curves using the centrifuge technique and linked with detailed anatomical observations in stems using light microscopy and transmission electron microscopy. The data show significant differences in stem P_{50} , varying twofold from -1.58 MPa in the Cape Verde Island accession to -3.07 MPa in the woody *soc1ful* double mutant. Out of all the anatomical traits measured, intervessel pit membrane thickness (T_{PM}) best explains the differences in P_{50} , as well as P_{12} and P_{88} . The association between embolism resistance and T_{PM} can be functionally explained by the air-seeding hypothesis. There is no evidence that the correlation between increased woodiness and increased embolism resistance is directly related to functional aspects. However, we found that increased woodiness is strongly linked to other lignification characters, explaining why mechanical stem reinforcement is indirectly related to increased embolism resistance. In conclusion, the woodier or more lignified accessions are more resistant to embolism than the herbaceous accessions, confirming the link between increased stem lignification and increased embolism resistance as also observed in other lineages. Intervessel pit membrane thickness, and to a lesser extent theoretical vessel implosion resistance and vessel wall thickness, are the missing functional links between stem lignification and embolism resistance.

Keywords: *Arabidopsis thaliana*, embolism resistance, herbaceous species, intervessel pit membrane, lignification, stem anatomy, xylem hydraulics.

Introduction

Long-distance water transport in the xylem connecting roots to leaves is essential for plant survival and distribution (Sperry, 2003; Brodribb, 2009; Lucas *et al.*, 2013; Lens *et al.*, 2016; Trueba *et al.*, 2017; Choat *et al.*, 2018; Brodribb *et al.*, 2020). Plants have developed an ingenious system to transport water upwards against gravity by a largely passive mechanism that is driven by a difference in negative xylem pressure created in the leaf mesophyll cell walls, known as the cohesion-tension theory (Dixon and Joly, 1895; Pickard, 1981; Brown, 2013). However, this negative or subatmospheric pressure inside the water-conducting xylem conduits puts water in a metastable liquid state, making it vulnerable to heterogeneous cavitation: the transition from liquid water to vapour by spontaneous destabilization of the hydrogen bonds between water molecules at nucleating sites (Steudle, 2001; Wheeler and Stroock, 2008; Brown, 2013; Venturas *et al.*, 2017). Under drought stress conditions, the xylem pressure becomes more negative, thereby increasing the risk of tiny vapour bubbles enlarging into a large embolism that blocks the water transport inside a conduit (Sperry and Tyree, 1988; Tyree and Zimmermann, 2002; Cochard, 2006). This embolized conduit can then cause gas bubbles to spread towards adjacent water-filled conduits via tiny pores in the interconduit pit membranes, a process called air-seeding. Air-seeding may lead to a rapid spread of drought-induced embolism throughout the plant, giving rise to hydraulic failure, i.e. a catastrophic loss of xylem hydraulic conductance, ultimately causing plant death (Brodribb and Cochard, 2009; Allen *et al.*, 2010; Urli *et al.*, 2013; Brodribb *et al.*, 2016, 2020; Anderegg *et al.*, 2016; Adams *et al.*, 2017; Kaack *et al.*, 2019; Zhang *et al.*, 2020). Acquiring a sufficient level of embolism resistance, therefore, represents one of the most essential adaptations for plant survival under drought conditions, along with other strategies such as reduced water-loss, increased water storage or root depth (Lens *et al.*, 2013; Gleason *et al.*, 2014; Martin-StPaul *et al.*, 2017; Billon *et al.*, 2020).

The relationship between the decline in hydraulic conductivity due to embolism and xylem pressure is plotted in a so-called vulnerability curve (VC), from which the pressure inducing 50% loss of hydraulic conductivity (P_{50}) – the often-cited proxy for drought tolerance – is derived (Maherali *et al.*, 2004; Choat *et al.*, 2012; Venturas *et al.*, 2017). Hydraulic studies show

Chapter 2: Intervessel pit membrane thickness and embolism resistance

a wide range of P_{50} across species (from -0.5 MPa to -20 MPa), and species occupying dry habitats are generally more resistant to embolism formation (more negative P_{50}) than species from wet habitats (Brodribb and Hill, 1999; Choat *et al.*, 2012; Larter *et al.*, 2015; Lens *et al.*, 2016; Trueba *et al.*, 2017). Xylem physiologists have measured P_{50} values in stems of over 2000 tree and shrub species. However, hydraulic measurements in herbaceous species are limited to only a few dozen species, despite the fact that a majority of our important food crops are herbs (Stiller, 2002; Holloway-Phillips and Brodribb, 2011; Lens *et al.*, 2013, 2016; Nolf *et al.*, 2016; Skelton *et al.*, 2017; Ahmad *et al.*, 2018; Dória *et al.*, 2018; Volaire *et al.*, 2018; Lamarque *et al.*, 2020; Bourbia *et al.*, 2020; Corso *et al.*, 2020). Therefore, it is essential to focus more on herb hydraulics and integrate these hydraulic traits in models that predict annual crop yields to consider the effects of drought and heatwave events (Asseng *et al.*, 2015).

In this paper, we focus on the model species *Arabidopsis thaliana* (L.) Heynh. This small herbaceous species is able to produce a limited amount of wood in the hypocotyl and at the base of the inflorescence stem (Chaffey *et al.*, 2002; Ko *et al.*, 2004; Nieminen *et al.*, 2004; Melzer *et al.*, 2008; Lens *et al.*, 2012). Wood formation can be moderately induced in wild-type accessions by either delaying flowering time under short days (Tixier *et al.*, 2013) or by clipping developing flowers (Chaffey *et al.*, 2002), by applying weights on the inflorescence stem (Ko *et al.*, 2004), or by increasing auxin levels (Agusti *et al.*, 2011; Brackmann *et al.*, 2018). A more extensive wood cylinder can be induced by modifying gene regulation that turns the herbaceous phenotype into a shrubby phenotype (Melzer *et al.*, 2008; Karami *et al.*, 2020), although this woodiness does not extend towards the upper parts of the inflorescence stems (Lens *et al.*, 2012). Since increased woodiness or lignification levels in stems have been linked to higher levels of embolism resistance in various plant groups (Tixier *et al.*, 2013; Lens *et al.*, 2013, 2016; Dória *et al.*, 2018, 2019), we selected three herbaceous wild-type accessions of *A. thaliana* with a different growth type and drought response (Columbia (Col-0), Cape Verde Islands (Cvi) and Shahdara (Sha); Bac-Molenaar *et al.*, 2016; Thoen *et al.*, 2017) and one woody mutant established in the Col-0 background (*soc1ful* knockout; Melzer *et al.*, 2008) to evaluate this potential correlation more closely. To this end, we applied the cavitron centrifuge method (Cochard *et al.*, 2013) to compare the xylem embolism resistance of inflorescence stems amongst the four accessions,

and assessed which xylem anatomical traits underlie the differences observed in P_{50} using detailed anatomical observations with light microscopy (LM) and transmission electron microscopy (TEM). Various hydraulically relevant stem traits were observed, such as the proportion of stem woodiness/lignification, intervessel pit membrane thickness, fiber wall thickness, theoretical vessel implosion index, and vessel grouping index (Table 1). We hypothesize that woodier or more lignified *Arabidopsis* stems are more resistant to embolism formation than less lignified stems and that this difference in embolism resistance is functionally driven by intervessel pit membrane thickness.

Materials and methods

Plant material

Three accessions and one woody mutant of *Arabidopsis thaliana* were chosen based on their contrasting growth form, the difference in drought tolerance and the minimum length of their inflorescence stems: (1) Columbia (Col-0, a direct descendant of Col-1 from Poland and Eastern Germany; Koornneef and Meinke, 2010; Passardi *et al.*, 2007; Somssich, 2019); (2) Shahdara (Sha, native to a low precipitation area of Shakhdarah valley, Tajikistan; Khurmatov, 1982; Trontin *et al.*, 2011); (3) Cape Verde Islands (Cvi, native to the high altitude region above 1,200 m on Cape Verde Islands; Lobin, 1983; Monda *et al.*, 2011); and (4) Col-0 accession in which two flowering time control genes *SUPPRESSOR OF OVEREXPRESSION OF CO 1* (*SOC1*) and *FRUITFULL* (*FUL*) are knocked out (*soc1ful* in Col-0 background; Melzer *et al.*, 2008). The three wild-type accessions were selected based on the length of their inflorescence stems (at least 30 cm required for the cavitron measurements, which exceeds by far the maximum vessel length of Col-0 reaching only 4 cm according to Tixier *et al.* (2013), to avoid potential open-vessel artefacts (Cochard *et al.*, 2013)), their differences in drought response (Bac-Molenaar *et al.*, 2016; Thoen *et al.*, 2017) and growth form. The *soc1ful* knockout was selected as the woody counterpart because of its extended levels of wood formation at the base of the inflorescence stems (Lens *et al.*, 2012). One hundred individuals from three accessions and one double knockout were grown from seeds sown directly in a mixture of soil and sand (4.5:1). After seed germination (10-12 days after sowing), the healthy seedlings were transferred and grown individually in 8 cm-diameter

Chapter 2: Intervessel pit membrane thickness and embolism resistance

pots in a growth chamber under controlled conditions of 20°C temperature and 16-h photoperiod, with 100 $\mu\text{mol m}^{-2} \text{s}^{-1}$ light intensity. Relative humidity (RH) was maintained at 70%. We synchronized the harvesting time for the four accessions, meaning that each accession was harvested at different ages (55-65 days for WT accessions, 80-90 days for *soc1ful*), depending on the time required for flowering and inflorescence stem development.

Xylem vulnerability to embolism

Sample preparation of inflorescence stems

The plants were harvested – with roots, leaves and flowers still attached – in the growth chamber facilities at the Institute of Biology Leiden (Leiden University, The Netherlands). The basal part of the inflorescence stems of each accession was cut underwater with a sharp razor blade into a length at least of 30 cm, and then immediately wrapped in wet tissues, enclosed in plastic bags, and shipped to the PHENOBOIS platform (INRAE, University of Bordeaux, France) for the hydraulic experiments that were carried out within a week of harvest. Before running the cavitron centrifuge measurements, the samples were recut underwater to a standard length of 27 cm, after which both ends were trimmed to fit the cavitron rotor. All siliques, leaves and flowers were removed from the stems just before the measurement.

Cavitron centrifuge method

Centrifugal force has been used to induce cavitation in stem segments by lowering the xylem pressure in the middle part of stems during spinning (Cochard, 2002; Cochard *et al.*, 2005). Vulnerability to embolism in the inflorescence stems was measured using ten individuals per vulnerability curve (VC) to generate sufficient hydraulic conductivity during the spinning experiment; about 10 VCs per accession were generated. A solution of deionized ultrapure water containing 1 mM CaCl_2 and 10mM KCl was used as a reference for the hydraulic conductivity measurements. The theoretically maximum hydraulic conductivity (K_{max} , $\text{m}^2 \text{MPa}^{-1} \text{s}^{-1}$) of the ten inflorescence stems was firstly calculated at near-zero MPa (low speed). The xylem pressure was then gradually decreased by -0.2 to -0.4 MPa for each

spinning step. The hydraulic conductivities at every rotation speed (K) were measured using Cavisoft software (Cavisoft v1.5, University of Bordeaux, France). The percentage loss of hydraulic conductivity (PLC) was computed as:

$$PLC = 100 \cdot (1 - (K/K_{MAX})) \quad (1)$$

The vulnerability curves were constructed and fitted with a sigmoid function (Pammenter and Van der Willigen, 1998) using NLIN procedure in SAS 9.4 (SAS 9.4; SAS Institute, Cary, NC, USA) following the equation:

$$PLC = 100 / [1 + \exp ((S/25) \cdot (P - P_{50}))] \quad (2)$$

where P_{50} represents the xylem pressure inducing 50% loss of hydraulic conductivity and S (% MPa⁻¹) is the slope of the VC at the inflexion point (P_{50}).

Stem anatomy

Sample preparation

Since the stem anatomy at the basal, more lignified part differs rather considerably compared to the middle part where the negative pressures were applied during the cavitron measurements, we made sections from both parts and performed the anatomical observations on the middle stem parts to match anatomy with P_{50} . From the 10 VCs we generated per accession, we selected three stems for three representative VCs (9 individuals per accession) for light microscopy (LM), and one stem for three representative VCs (3 individuals per accession) for transmission electron microscopy (TEM). The anatomical measurements (Table 1) were carried out using ImageJ (National Institutes of Health, Bethesda, USA) following the recommendations of (Scholz *et al.*, 2013).

Light microscopy (LM)

The inflorescence stems were cut into small pieces, ca 1 cm long and stored in 70% ethanol. Fixed samples were then infiltrated and embedded in LR-White resin (Hamann *et al.*, 2011). The embedded samples were sectioned using a Leica RM 2265 microtome with disposable Tungsten carbon blades (Leica, Eisenmark, Wetzlar, Germany) at a thickness of 4 μm . Subsequently, the sections were heat-fixed onto the slides with 40% acetone, stained with Toluidine blue (1% (w/v) toluidine blue (VWR chemical BDH®, Radnor, Pennsylvania, USA) in 1% (w/v) borax), rinsed with distilled water, air-dried, and mounted with DPX new-100579 mounting medium (Merck Chemicals B.V., Amsterdam, Northern Holland, The Netherlands). The anatomical features were observed under a Leica DM2500 light microscope and photographed with a Leica DFC-425 digital camera (Leica microscopes, Wetzlar, Germany). The diameter of vessels (D) was calculated as:

$$D = (\sqrt{4A}) / \pi \quad (3)$$

where D represents the diameter of vessels, and A is the conduit surface area. The hydraulically weighted vessel diameter (D_H) was calculated based on the diameter of vessels (D) following the equation (Tyree and Zimmermann, 2002):

$$D_H = (\sum D^4 / N)^{1/4} \quad (4)$$

where D is the diameter of vessels measured using equation 3 and N is the number of conduits measured. All the measurements are explained in Table 1.

Transmission Electron Microscopy (TEM)

After the cavitron experiment, 1 cm-long pieces from the middle part of the inflorescence stems were immediately collected and fixed in Karnovsky's fixative for 48 hr (Karnovsky, 1965). The samples were cleaned three times in 0.1M cacodylate buffer, then post-fixed with 1% buffered osmium tetroxide, rinsed again with buffer solution, stained with 1% uranyl acetate, and dehydrated in a series of ethanol: 1 % uranyl acetate

replacement, with increasing concentration of ethanol (30%, 50%, 70%, 96%, and twice in $\geq 99\%$). The samples were then infiltrated with Epon 812 n (Electron Microscopy Sciences, Hatfield, England) and placed at 60°C for 48 hr in the oven. The Epon blocks were trimmed into 2 μm -thick using a rotary microtome with a glass knife. Subsequently, the cross-sections with many vessel-vessel contact areas were cut into ultrathin sections of 90-95 nm using a Leica EM UC7 ultramicrotome with a diamond knife. The sections were dried and mounted on film-coated copper slot grids with Formvar coating (Agar Scientific, Stansted, UK), and post-stained with uranyl acetate and lead citrate. Ultrastructural observations of intervessel pits were performed and photographed using a JEM-1400 Plus TEM (JEOL, Tokyo, Japan), equipped with an 11 MPixel camera (Quemesa, Olympus). At least 25 relaxed, non-shrunken intervessel pit membranes were selected from 3 individuals per accession to observe intervessel pit membranes thickness and pit chamber depth (Table 1).

Statistical analysis

To assess the differences between embolism resistance among the four accessions studied, we performed General Linear Models (GLM). A Newman-Keuls post-hoc test was applied to test whether or not embolism resistance (P_{50}) and anatomical characters differ amongst accessions. We carried out multiple linear regression models based on non-standardized and standardized data from the middle part of the stem segments to evaluate which stem anatomical traits (predictive variables) best explain embolism resistance, with P_{50} , P_{12} (air entry point) and P_{88} as response variables. Predictors were firstly selected based on biological knowledge, followed by a collinearity analysis through pairwise scatterplots and variance inflation factor (VIF). To deduce the most parsimonious multiple linear regression model, we applied “step” function from “stats” package (R Core Team 2016; available in CRAN) to remove the least predictive variables each time according to Akaike Information Criterion (AIC). Robust fitting of linear models through iteratively reweighted least squares (IWLS) and MM estimation (M-estimation with Tukey’s bi-weight initialized by a specific S-estimator) was used to deal with the outliers and leverages. In addition, to assess the relative importance of the remaining explanatory variables of P_{50} , we calculated the relative importance of regressors in linear models. Pearson’s correlation analysis was applied to assess the correlation between

Chapter 2: *Intervessel pit membrane thickness and embolism resistance*

the predictive variables and P_{50} . We used R version 3.6.3 in R Studio version 1.2.5033 for all analyses. All the differences were considered significant when p-value was <0.05 .

Table 1 List with the anatomical characters measured with reference to their acronyms, definitions, calculations, microscope techniques, and units.

Acronyms	Definition	Calculation	Number of measurements	Unit	Technique
A _F	Fiber cell area	Area of single xylem fiber in cross-section	Min. 30 fibers	μm ²	LM
A _{FL}	Fiber lumen area	Area of single xylem fiber lumen in cross-section	Min. 30 fibers	μm ²	LM
A _{FW}	Fiber wall area	A _F - A _{FL} for the same fiber	Min. 30 fibers	μm ²	LM
A _{LIG}	Lignified stem area	Total xylem area + fiber caps area + lignified pith cell area in cross-section	9 stems per accession	mm ²	LM
A _{PITH}	Pith area	Total pith area in cross-section	9 stems per accession	mm ²	LM
A _S	Total stem area	Total stem area in cross-section	9 stems per accession	mm ²	LM
D	Diameter of vessels	Equation 3	Min. 50 vessels	μm	LM
D _H	Hydraulically weighted vessel diameter	Equation 4	Min. 50 vessels	μm	LM
D _{MAX}	Maximum vessel lumen diameter	Diameter of single vessel	Min. 30 vessels	μm	LM
D _{PC}	Pit chamber depth	Distance from the relaxed pit membrane to the inner pit aperture	Min. 25 pits	μm	TEM
P _{FWFA}	Proportion of fiber wall area per fiber cell area	A _{FW} /A _F for the same fiber; a measure of xylem fiber wall thickness	Min. 30 fibers	-	LM

Chapter 2: Intervessel pit membrane thickness and embolism resistance

Acronyms	Definition	Calculation	Number of measurements	Unit	Technique
P_{LIG}	Proportion of lignified area per total stem area	A_{LIG}/A_S	9 stems per accession	-	LM
T_{PM}	Intervessel pit membrane thickness	Thickness of intervessel pit membrane measured at its thickest point	Min. 25 measurements	μm	TEM
T_V	Vessel wall thickness	Thickness of a single vessel wall	Min. 30 Vessels	μm	LM
T_{VW}/D_{MAX}	Thickness-to-span ratio of vessels	Double intervessel wall thickness divided by the maximum diameter of the largest vessel	Min. 30 measurements	μm	LM
$(T_{VW}/D_{MAX})^2$	Theoretical vessel implosion resistance	$(T_{VW}/D_{MAX})^2$	Min. 30 measurements	-	LM
V_D	Vessel density	Number of vessels per mm^2	Min. 5 measurements	No. of vessels/ mm^2	LM
V_G	Vessel grouping index	Ratio of total number of vessels to total number of vessel groupings (incl. solitary and grouped vessels)	Min. 50 vessel groups	-	LM

Results

Xylem vulnerability to embolism amongst the Arabidopsis accessions

P_{50} of each accession is significantly different from each other and varied twofold across the accessions studied ($F = 57.70$; p -value < 0.001) from -1.58 MPa to -3.07 MPa (Figure 1). Amongst the four accessions, stems of the *soc1ful* double mutant are the most resistant to embolism ($P_{50} = -3.07 \pm 0.30$ (SD) MPa; Supplementary Table S1) with a slope of $62\% \text{ MPa}^{-1}$ (Figure 1a), followed by Sha ($P_{50} = -2.49 \pm 0.11$ MPa; slope = $59\% \text{ MPa}^{-1}$), Col-0 ($P_{50} = -2.14 \pm 0.18$ MPa; slope = $38\% \text{ MPa}^{-1}$), and Cvi ($P_{50} = -1.58 \pm 0.05$ MPa; slope = $142\% \text{ MPa}^{-1}$) (Supplementary Table S1; Figure 1a). The P_{50} variation within accessions is remarkably low except for *soc1ful* ranging from -2.59 MPa to -3.42 MPa (Figure 1b). Similar significant variation in P_{12} ($F = 26.79$; p -value < 0.001) is observed; for P_{88} , Col-0 and Sha are not significantly different from each other ($F = 34.8$; p -value = 0.517).

Stem anatomical traits amongst the accessions studied

The features that are significantly different from each other among the accessions studied are intervessel pit membrane (T_{PM}) ($F = 118.8$; p -value $< 2e^{-16}$; Supplementary Figure S1a; Figures 2c-d; Figures 3c-d), theoretical vessel implosion resistance $(T_{\text{VW}}/D_{\text{MAX}})^2$ ($F = 37.35$; p -value = $1.44e^{-10}$; Supplementary Figure S1b) and proportion of fiber wall area per fiber cell area (P_{FWFA}) ($F = 65.33$; p -value = $9.75e^{-14}$; Supplementary Figure S1c). Meanwhile, proportion of lignified area per total stem area (P_{LIG}) of Col-0 is different from *soc1ful* and Cvi ($F = 18.68$; p -value = $3.48e^{-07}$; Supplementary Figure S1d), which is similar to Sha. Furthermore, vessel grouping index (V_{G}) of Col-0 and Cvi is similar, which is also the case for Sha and *soc1ful*; V_{G} of both groups, however, are significantly different from each other ($F = 43.45$; p -value = $2.17e^{-11}$; Supplementary Figure S1e). Vessel wall thickness (T_{V}) of Col-0 and Cvi are different from each other, and different from Sha and *soc1ful* which have a similar T_{V} ($F = 33.46$; p -value = $5.52e^{-10}$; Supplementary Figure S1f).

Chapter 2: Intervessel pit membrane thickness and embolism resistance

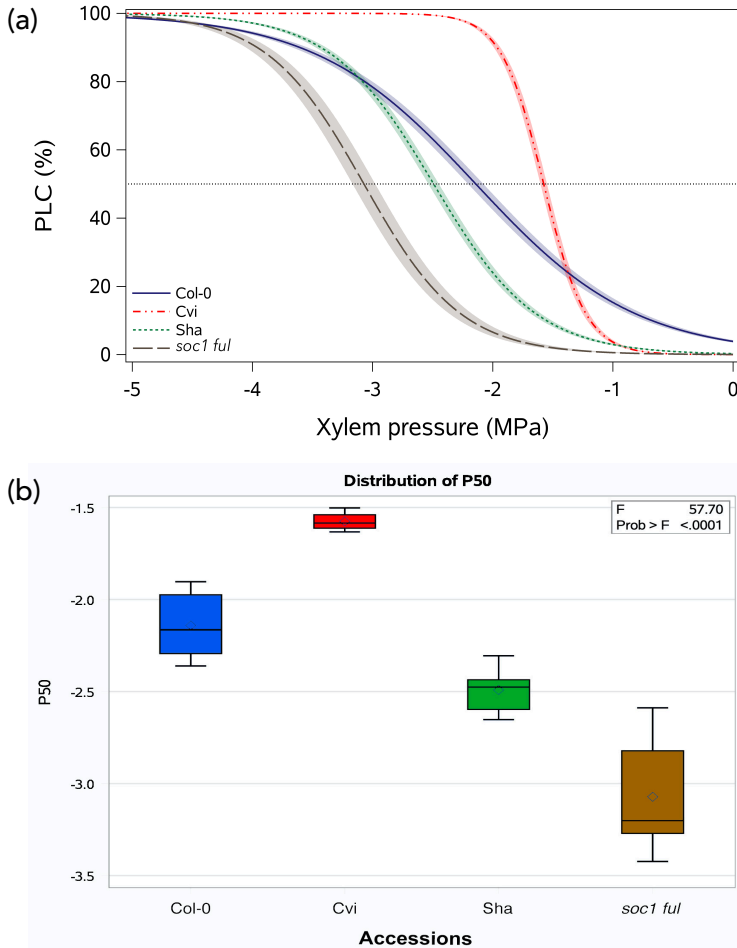


Figure 1 Stem P_{50} is significantly different across *A. thaliana* accessions. (a) mean vulnerability curves (VCs) for each accession presents the percentage loss of conductivity (PLC) as a function of xylem pressure (MPa). The dotted line shows 50% loss of conductivity (P_{50}). Shaded bands represent standard errors based on ca. 10 VCs per accession.; (b) boxplot showing P_{50} distribution and variation within and between accessions (p -value = 0.05).

Relationship between embolism resistance and anatomical features

Both T_{PM} and $(T_{VW}/D_{MAX})^2$ strongly correlated positively with embolism resistance based on a Pearson correlation test ($r = -0.93$, p -value = $3.1e^{-16}$; $r = -0.88$, p -value = $2.1e^{-12}$, respectively; Figures 4b-c). Furthermore, there are correlations between embolism resistance and vessel wall thickness (T_V) ($r = -0.86$, p -value = $2.5e^{-11}$; Supplementary Figure S2a), between embolism resistance and vessel grouping index (V_G) ($r = -0.77$, p -value = $3.6e^{-08}$; Supplementary Figure S2b), between embolism resistance and proportion of lignified area per total stem area (P_{LIG}) ($r = -0.67$, p -value = $7.2e^{-06}$; Supplementary Figure S2c), and between embolism resistance and proportion of fiber wall per fiber cell area (P_{FWFA}) ($r = -0.73$, p -value = $3.4e^{-07}$; Supplementary Figure S2d). Multiple regression analysis with robust fitting shows that the best predictors explaining P_{50} variation are the thickness of intervessel pit membrane (T_{PM} ; Figures 2c-d, 3c-d) and theoretical vessel implosion resistance ($(T_{VW}/D_{MAX})^2$), followed by vessel wall thickness (T_V), and vessel grouping index (V_G) ($R^2 = 0.9468$, p -value $< 2.2e^{-16}$) (Table 2). However, only T_{PM} and $(T_{VW}/D_{MAX})^2$ are highly significant in this model (p -value < 0.01) (Table 2). According to the regressor analysis, the relative importance of T_{PM} and $(T_{VW}/D_{MAX})^2$ in explaining P_{50} variation is 31% and 25%, respectively (Table 2, Figure 4a). The proportion of lignified area per total stem area (P_{LIG}) does not explain embolism resistance based on the most parsimonious multiple regression model (AIC score = -134.39; Table 2, Supplementary Table S2), but is included in the second most parsimonious model (AIC = -132.44; Supplementary Table S3).

Correspondingly, T_{PM} also best explains P_{12} and P_{88} variations based on multiple regression models, followed by pit chamber depth (D_{PC}) ($R^2 = 0.9507$, p -value $< 2.2e^{-16}$, $R^2 = 0.8646$, p -value $< 3.88e^{-13}$, respectively) (Supplementary Tables S4, S5). In addition, theoretical vessel implosion resistance ($(T_{VW}/D_{MAX})^2$) is included in P_{88} multiple regression model (p -value < 0.05) (Supplementary Tables S5), while T_V is included in the P_{12} multiple regression model as a significant predictor (p -value < 0.001) (Supplementary Tables S4). Correlations between the anatomical variables are the following: thickness of intervessel pit membrane is strongly correlated to theoretical vessel implosion resistance, vessel wall thickness, vessel grouping, and proportion of fiber wall per fiber cell area ($r = 0.77, 0.76, 0.72$, and 0.68 , respectively; p -value < 0.001) (Supplementary Figure S3). Apart from that,

Chapter 2: Intervessel pit membrane thickness and embolism resistance

$(T_{VW}/D_{MAX})^2$ correlates with T_V , V_G , and P_{FWFA} ($r = 0.77, 0.62$, and 0.59 , p -value < 0.001), V_G is correlated with T_V ($r = 0.63$; p -value < 0.001) (Supplementary Figure S3), and P_{LIG} shows correlations with T_{PM} , V_G , $(T_{VW}/D_{MAX})^2$ and T_V ($r = 0.67, 0.66, 0.58$ and 0.58 , respectively; p -value < 0.001 ; Supplementary Figure S3).

Table 2 The best multiple regression model, based on AIC scores, of anatomical features explaining P_{50} variation in stems of the four *Arabidopsis thaliana* accessions studied.

Predictors	Estimate	Std. Error	z value	Pr ($> z $)
(Intercept)	0.901	0.315	2.858	0.004262
T_{PM}	-10.896	2.035	-5.356	8.522E-08***
$(T_{VW}/D_{MAX})^2$	-35.174	10.927	-3.219	0.001287*
T_V	-0.516	0.239	-2.163	0.031*
V_G	-0.280	0.183	-1.529	0.126

T_{PM} = intervessel pit membrane thickness; $(T_{VW}/D_{MAX})^2$ = theoretical vessel implosion resistance; T_V = vessel wall thickness; V_G = vessel grouping index; *** p -value < 0.001 ; ** p -value < 0.01 ; * p -value < 0.05

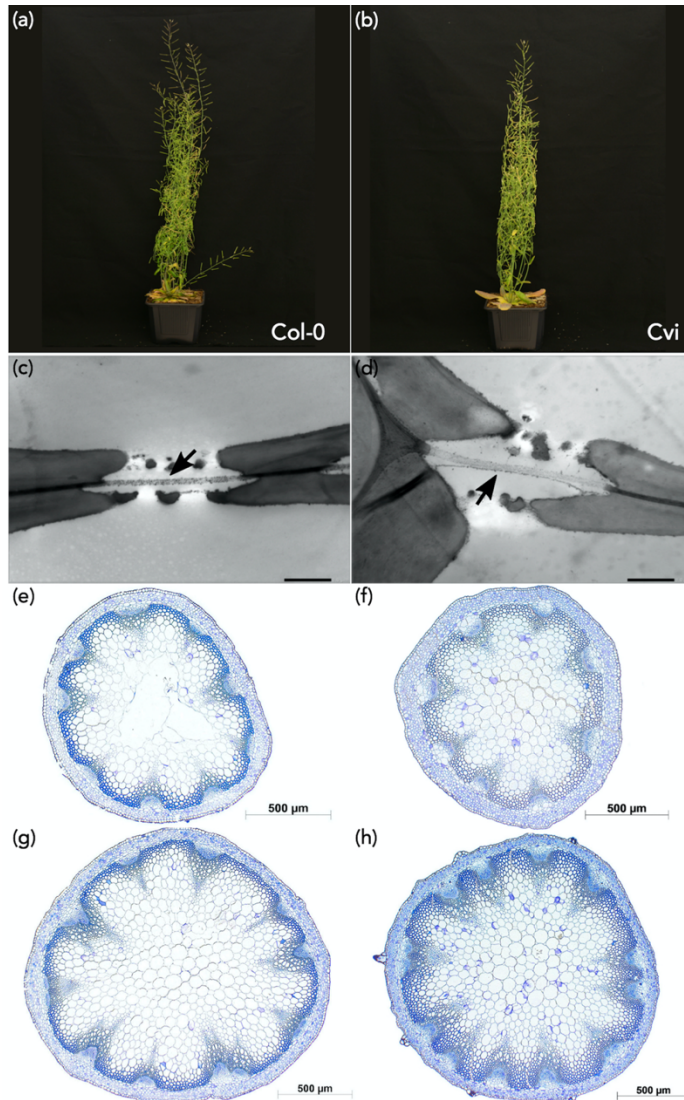


Figure 2 Illustration of growth form and cross-sections of inflorescence stems of Col-0 (left, 57 days after sowing) and Cvi (right, 57 days after sowing). (a, b) growth form; (c, d) transmission electron microscope images of intervessel pit membranes (arrows); (e, f) light microscope images of the cross-section at the middle part of inflorescence stems; (g, h) light microscope images of the cross-section at the basal part of inflorescence stems. Scale bars represent 1 μm (c-d), or 500 μm (e-h).

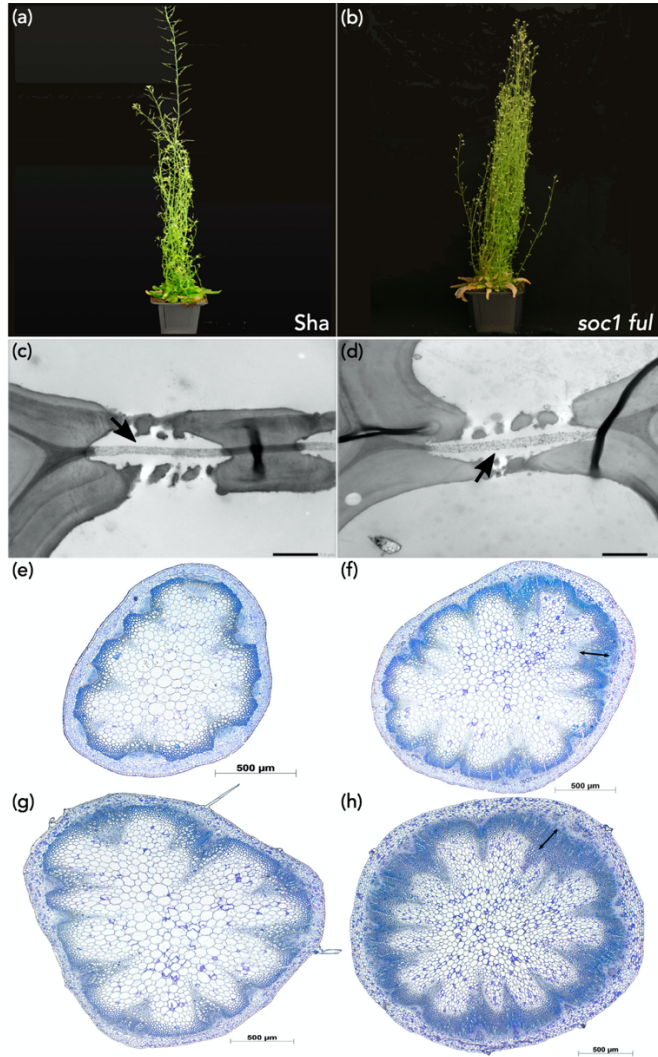


Figure 3 Illustration of growth form and cross-sections of inflorescence stems of Sha (left, 57 days after sowing) and *soc1ful* (right, 80 days after sowing). (a, b) growth form; (c, d) transmission electron microscope images of intervessel pit membranes (arrows); (e, f) light microscope images of the cross-section at the middle part of inflorescence stems, the double-pointed arrow shows the wood cylinder; (g, h) light microscope images of the cross-section at the basal part of inflorescence stems, the double-pointed arrow shows the wood cylinder. Scale bars represent 1 μm (c-d), 500 μm (e-h).

Discussion

We found a twofold variation in stem P_{50} amongst the *Arabidopsis thaliana* accessions studied (ranging from -1.5 to -3.0MPa; Figure 1), which is significantly associated with an increase in the thickness of the intervessel pit membrane (T_{PM} ; Figure 4) and is in line with the air-seeding hypothesis. Our findings confirm earlier reports that *Arabidopsis* inflorescence stems with increased levels of lignification are better able to avoid drought-induced embolism than stems that are less lignified (Figures 2-3), which is based on (1) a more elaborate set of wild-type accessions (three vs one), (2) multiple vulnerability curves (VCs) per accession compared to only one VC per accession, and (3) more detailed anatomical observations compared to previous structure-function papers in *Arabidopsis* (Lens *et al.*, 2013; Tixier *et al.*, 2013). We investigated correlations amongst a range of anatomical traits related to stem lignification and uncovered statistical associations between increased lignification vs T_{PM} and between vessel wall thickness vs T_{PM} . Our comparative approach suggests an indirect link between traits related to mechanical strength in stems and P_{50} , with T_{PM} serving as the missing functional link between stem reinforcement and vulnerability to embolism.

Variation in stem P_{50} amongst Arabidopsis accessions agrees with other herbs and is best explained by intervessel pit membrane thickness (T_{PM})

Our embolism resistance measurements with the cavitron technique support earlier papers reporting values for the same species based on the more traditional centrifuge technique in combination with a portable water flow device (XYL'EM) (from -2.25 to -3.5 MPa; Lens *et al.*, 2013; Tixier *et al.*, 2013). Our data also fall within the range of the published P_{50} values for herbaceous eudicot species (Tyree *et al.*, 1986; Stiller, 2002; Saha *et al.*, 2009; Li *et al.*, 2009; Rosenthal *et al.*, 2010; Nolf *et al.*, 2014; Skelton *et al.*, 2017; Dória *et al.*, 2018, 2019; Bourbia *et al.*, 2020), although more negative P_{50} values (up to -7.5 MPa) of herbaceous stems, especially in grasses, have been reported in some papers (Lens *et al.*, 2016; Volaire *et al.*, 2018). Amongst the anatomical traits we observed, T_{PM} strongly correlates with P_{50} and explains best the variation in P_{50} observed based on a statistical test showing the relative importance of regressors in our most parsimonious multiple linear regression model (Table 2; Figures 4a-b). Our observations in *Arabidopsis* fit well with other published data of woody and herbaceous

Chapter 2: Intervessel pit membrane thickness and embolism resistance

species where properly fixated intervessel pit membranes have been measured in stems that were subjected to P_{50} measurements (Li *et al.*, 2016; Dória *et al.*, 2018, 2019; Supplementary Figure S4).

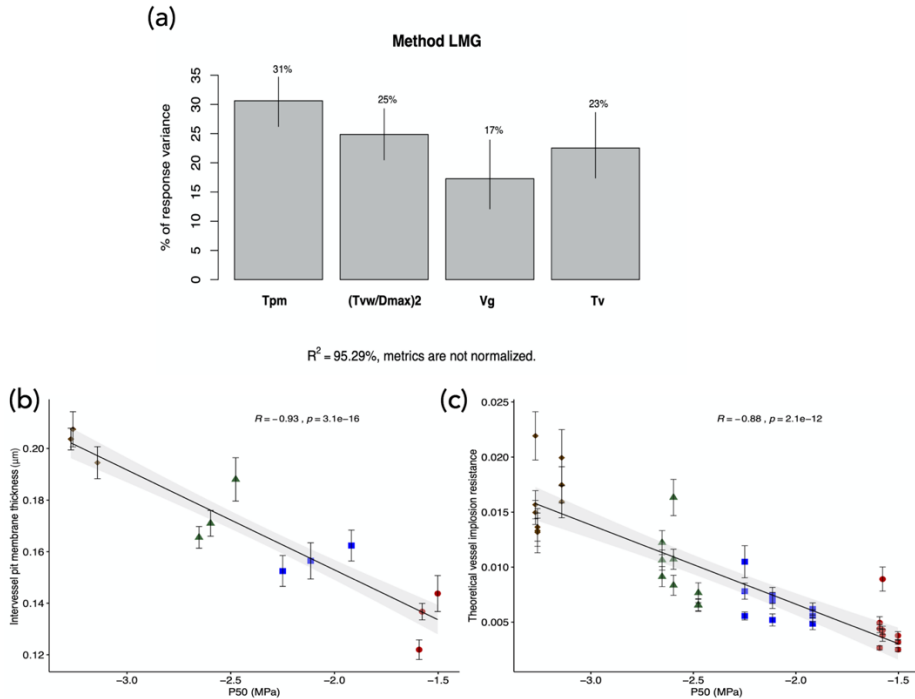


Figure 4 The relative importance and correlations of intervessel pit membrane thickness and theoretical vessel implosion resistance to P_{50} (a) Relative importance of P_{50} variation is mainly explained by intervessel pit membrane thickness (T_{PM}) and theoretical vessel implosion resistance $(T_{VW}/D_{MAX})^2$ based on R^2 contribution averaged over orderings among regressors; (b) negative correlation between thickness of intervessel pit membrane (T_{PM}) and P_{50} ; (c) negative correlation between theoretical vessel implosion resistance $(T_{VW}/D_{MAX})^2$ and P_{50} . Colours and styles refer to the accession studied: Col-0 (blue-filled square), Cvi (red-filled circle), Sha (green-filled triangle) and *soc1ful* (brown-filled diamond).

Furthermore, intervessel pit membrane thickness is the only trait that is also significant in the P_{12} and P_{88} multiple regression models, which emphasizes the functional relevance of T_{PM} in our dataset (Supplementary Tables S4, S5). As highlighted before, this T_{PM} – P_{50} correlation is undoubtedly functionally relevant because it nicely fits with the air-seeding mechanism. Although we do not fully understand exactly how this mechanism works at the ultrastructural level, the oversimplified 2D view suggesting that air-

seeding occurs via the single largest pit membrane pore should be abandoned (Wheeler *et al.*, 2005). Instead, a more realistic 3D structure of intervessel pit membranes shows that a single pit membrane pore – being highly interconnected with other pores – has multiple constrictions that are often narrower than 50 or 20 nm when pit membranes are thinner or thicker than 300 nm, respectively (Zhang *et al.*, 2020). In other words, the chance of having a smaller pore constriction becomes higher with thicker pit membranes as this elongates the multiconstriction pit membrane pore. Consequently, air-seeding is not determined by the single largest pore in a pit membrane, but by the minimum constriction across all the interconnected pores in a given pit membrane (Kaack *et al.*, 2019; Zhang *et al.*, 2020). This explains why species with thicker intervessel pit membranes are better able to withstand air bubble spread between adjacent conduits under drought conditions than species with thinner intervessel pit membranes (Jansen *et al.*, 2009; Li *et al.*, 2016; Dória *et al.*, 2018). However, more ultrastructural observations of intact pit membranes and the role of surface-active substances such as phospholipids in the xylem sap and pit membranes should be carried out to improve our understanding of air bubble formation and spread at the ultrastructural level (Schenk *et al.*, 2017, 2018; Zhang *et al.*, 2020).

Disentangling the correlation between traits impacting mechanical strength and embolism resistance

Based on Pearson's correlation test, the proportion of lignified area per total stem area (P_{LIG}) is significantly correlated to P_{50} (Supplementary Data Figures S2c, S3). This is in line with our previous results in *Arabidopsis* (Lens *et al.*, 2013), in other lineages of Brassicaceae and Asteraceae (Dória *et al.*, 2018, 2019), and in grasses (Lens *et al.*, 2016) showing that more woody/lignified stems are more resistant to embolism formation compared to close relatives with less woody/lignified stems. However, P_{LIG} is not included in the most parsimonious multiple regression P_{50} model (Table 2); it is retained in the second most parsimonious model (Supplementary Table S3), though, explaining only 10% of the P_{50} variation (results not shown). Consequently, in our dataset, P_{LIG} is not a key functional trait contributing to vulnerability to embolism in stems of the *Arabidopsis* accessions studied. Still, it does have predictive value due to its correlation with other traits that are considered to be more relevant. Interestingly, P_{LIG} is significantly

Chapter 2: Intervessel pit membrane thickness and embolism resistance

correlated to several other lignification traits, of which intervessel pit membrane thickness (T_{PM}), theoretical vessel implosion resistance (T_{VW}/D_{MAX})² and vessel wall thickness (T_V) are prime examples (Supplementary Figure S3). These three traits explain altogether, 79% of the P_{50} variation in the most parsimonious multiple regression model (Figure 4a). When comparing the three P_{12} - P_{50} - P_{88} multiple regression models, it is interesting to note that the depth of pit chamber (D_{PC}) is absent in the P_{50} model (Table 2) but pops up as highly significant in both P_{12} - P_{88} models (Supplementary Tables S4, S5). It is hypothesized that shallower pit chambers minimize interconduit pit membrane stretching during aspiration and thereby reducing the mechanical stresses on the membranes in both angiosperms as gymnosperms (Hacke and Jansen, 2009; Lens *et al.*, 2011). However, D_{PC} does not seem to be generally correlated with embolism resistance across all lineages observed (Dória *et al.*, 2018).

The (indirect) correlation between P_{50} and traits impacting mechanical strength has also been highlighted in other studies that have found links between embolism resistance vs thickness-to-span ratio of conduits (Hacke *et al.*, 2001; Bouche *et al.*, 2014), vs vessel wall thickness (Jansen *et al.* 2009; Li *et al.* 2016; see also next paragraph), vs wood density (Jacobsen *et al.*, 2005; Hoffmann *et al.*, 2011; Anderegg *et al.*, 2016; Gleason *et al.*, 2016), vs fiber wall thickness (Jacobsen *et al.*, 2005, 2007), vs lignin content (Pereira *et al.*, 2018), and vs lignin composition (Awad *et al.*, 2012; Lima *et al.*, 2018). Out of all these lignification characters, vessel wall reinforcement for a given lumen area – expressed either as thickness-to-span ratio of vessels or theoretical vessel implosion resistance – explains 25% of the P_{50} variation (Figure 4a), but only 3% of the P_{88} variation (results not shown), and could potentially present a secondary functional link due to its direct association with the long-distance water flow in plants that is prone to negative pressures. Also, in conifers, the pressure causing conduit implosion is correlated with embolism resistance, but it is more negative than P_{50} for most species. Since vessel collapse due to negative pressures has never been observed in woody nor herbaceous stems, it suggests that embolism occurs before the critical vessel implosion threshold is reached (Choat *et al.*, 2012; Bouche *et al.*, 2014), which is likely also the case for herbaceous species. Only a few reports of (reversible) vessel collapse in the smallest leaf veins are reported, which could be a mechanism to prevent embolism upstream in the major veins (Zhang *et al.*, 2016).

Variation in theoretical vessel implosion resistance ($(T_{VW}/D_{MAX})^2$) among *Arabidopsis thaliana* stems studied is mainly determined by the changes of vessel wall thickness (T_V), explaining 64% of the variation, whereas the maximum vessel lumen diameter (D_{MAX}) only accounts for 31% (Supplementary Figure S5). This result is in line with Bouche *et al.* (2014), who found that T_V drives the variation in T_{VW}/D_{MAX} , suggesting that species tend to mechanically reinforce their conduits by increasing wall thickness instead of reducing conduit size in order to maintain a minimum level of hydraulic conductance. But, at the same time, T_V also positively correlates with T_{PM} (Supplementary Figure S3), with thicker vessel walls leading to thicker intervessel pit membranes (Jansen *et al.*, 2009) and thus higher embolism resistance (T_V explaining 23% of the P_{50} variation (Figure 4a) and 18% of the P_{12} variation (results not shown)). On the other hand, other studies investigating the driver for T_{VW}/D_{MAX} variation found that D_{MAX} is more important (Pittermann *et al.*, 2006; Sperry *et al.*, 2006), thereby reducing the relevance of conduit wall thickening. Vessel grouping (V_G), the final anatomical variable in the multiple regression P_{50} model, is the only character independent from lignification, and only accounts for 17% of the variation (Figure 4a) and 5% of the P_{88} variation. Pearson's correlation analysis shows a significant positive correlation between V_G and embolism resistance. Increased vessel connectivity safeguards all pathways in the 3D vessel network when only one vessel in a vessel multiple is embolized (Carlquist, 1984; Lens *et al.*, 2011). This can only work when the intervessel pit membranes are sufficiently thick to isolate the embolisms in a given vessel multiple at a normal drought stress level, which seems to be the case in *Arabidopsis*. If T_{PM} is too thin, greater vessel connectivity increases the probability of embolism spreading via air-seeding, potentially leading to lethal levels of hydraulic failure (Tyree and Zimmermann 2002; Loepfe *et al.*, 2007; Johnson *et al.*, 2020).

Chapter 2: Intervessel pit membrane thickness and embolism resistance

In conclusion, we found a twofold difference in stem P_{50} across the *Arabidopsis* accessions studied, with the woody mutant (*soc1ful*) being most resistant to embolism compared to the wild-type accessions. This confirms earlier studies that found a link between increased stem lignification and increased embolism resistance in *Arabidopsis* and other lineages. However, a higher degree of stem lignification cannot functionally explain the pattern observed, and therefore has to co-evolve with traits that functionally impact P_{50} . Intervessel pit membrane thickness (T_{PM}), and to a lesser extent theoretical vessel implosion resistance ($(T_{VW}/D_{MAX})^2$), vessel wall thickness (T_V) and pit chamber depth (D_{PC}), are strongly correlated with vulnerability to embolism and contribute most to the P_{12} - P_{50} - P_{88} variation observed, making T_{PM} the main functional missing link between stem lignification and embolism resistance. Adding more accessions and performing complementary measurements related to drought tolerance in stems, leaves and roots will undoubtedly shed more light into the complex mechanism that this short-lived, herbaceous model species has developed in order to cope with periods of water shortage.

Acknowledgements

We thank Gaëlle Capdeville, Regis Burrett, Anne-Isabelle Gravel and Laurent Lamarque for technical support. We also acknowledge the statistical support of Pablo Cisneros Araujo. This work is funded by a PhD scholarship awarded to AT from the Institute for the Promotion of Teaching Science and Technology (IPST), Thailand, and by the Dutch Research Council NWO (grant number ALWOP.488)

Supplementary data

Table S1 P_{50} and anatomical traits measured (mean \pm SD) of the four *Arabidopsis thaliana* accessions.

Traits/ accessions	Col-0	Cvi	Sha	<i>soc1ful</i>
P_{50}	-2.14 \pm 0.18	-1.58 \pm 0.05	-2.49 \pm 0.11	-3.07 \pm 0.30
P_{LIG} (middle part of stem)	0.175 \pm 0.001	0.193 \pm 0.016	0.210 \pm 0.009	0.252 \pm 0.013
T_{PM} (μ m)	0.157 \pm 0.005	0.134 \pm 0.011	0.175 \pm 0.012	0.202 \pm 0.007
D_{PC} (μ m)	0.438 \pm 0.015	0.357 \pm 0.017	0.400 \pm 0.010	0.353 \pm 0.022
D (μ m)	20.954 \pm 0.154	22.577 \pm 1.202	20.714 \pm 1.211	20.036 \pm 2.155
D_H (μ m)	21.995 \pm 0.189	23.456 \pm 1.384	21.403 \pm 1.127	20.625 \pm 1.967
D_{MAX} (μ m)	25.992 \pm 0.828	23.854 \pm 0.744	25.837 \pm 2.834	21.562 \pm 0.870
T_V	0.996 \pm 0.048	0.723 \pm 0.082	1.179 \pm 0.133	1.284 \pm 0.045
$(T_{VW}/D_{MAX})^2$	0.007 \pm 0.001	0.004 \pm 0.001	0.010 \pm 0.003	0.016 \pm 0.002
P_{FWFA}	0.528 \pm 0.063	0.397 \pm 0.049	0.786 \pm 0.047	0.671 \pm 0.045
V_D	116.444 \pm 5.251	102.706 \pm 9.753	120.756 \pm 14.931	127.756 \pm 10.735
V_G	1.782 \pm 0.057	1.829 \pm 0.115	2.329 \pm 0.108	2.342 \pm 0.050

P_{LIG} = proportion of lignified area per total stem area; T_{PM} = intervessel pit membrane thickness; D_{PC} = pit chamber depth; D = vessel diameter; D_H = hydraulically weighted vessel diameter; D_{MAX} = maximum vessel diameter; T_V = vessel wall thickness; $(T_{VW}/D_{MAX})^2$ = theoretical vessel implosion resistance; P_{FWFA} = proportion of fiber wall area per fiber cell area; V_D = vessel density; V_G = vessel grouping index

Chapter 2: Intervessel pit membrane thickness and embolism resistance

Table S2 The most parsimonious multiple regression model with standardized data of anatomical features explaining P_{50} variation in stems of the four *Arabidopsis thaliana* accessions studied.

Predictors	Estimate	Std. Error	z value	Pr (> z)
(Intercept)	-1.237988	0.079647	-15.5435	< 2.2E-16
T_{PM}	-0.931430	0.173915	-5.3557	8.524E-08***
$(T_{VW}/D_{MAX})^2$	-0.683314	0.212280	-3.2189	0.001287**
T_V	-0.533092	0.246432	-2.1632	0.030522*
V_G	-0.274562	0.179581	-1.5289	0.126288

T_{PM} = intervessel pit membrane thickness; $(T_{VW}/D_{MAX})^2$ = theoretical vessel implosion resistance; T_V = vessel wall thickness; V_G = vessel grouping index; *** p -value < 0.001; ** p -value < 0.01; * p -value < 0.05

Table S3 Second most parsimonious multiple regression model of anatomical features explaining P_{50} variation in stems of the four *Arabidopsis thaliana* accessions studied, including proportion of lignified area per total stem area (P_{LIG}).

Predictors	Estimate	Std. Error	z value	Pr ($> z $)
(Intercept)	0.902453	0.321147	2.81010	0.004953
T_{PM}	-10.94886	2.29588	-4.76890	1.852E-06***
$(T_{VW}/D_{MAX})^2$	-35.08942	11.41948	-3.07280	0.002121**
T_V	-0.51645	0.25839	-1.99870	0.045636*
V_G	-0.28617	0.19144	-1.49480	0.134960
P_{LIG}	0.09505	1.28027	0.07420	0.940816

T_{PM} = intervessel pit membrane thickness; $(T_{VW}/D_{MAX})^2$ = theoretical vessel implosion resistance; T_V = vessel wall thickness; V_G = vessel grouping index; P_{LIG} = proportion of lignified area per total stem area; *** p -value < 0.001; ** p -value < 0.01; * p -value < 0.05

Table S4 The best multiple regression model, based on AIC scores, of anatomical features, explaining P_{12} variation in stems of the four *Arabidopsis thaliana* accessions studied.

Predictors	Estimate	Std. Error	z value	Pr (> z)
(Intercept)	-1.84631	0.52630	-3.50810	0.0004513
T_{PM}	-25.44504	2.57654	-9.87560	< 2.2E-16***
P_{FWFA}	0.73844	0.52827	1.39790	0.1621552
T_V	-0.80998	0.22178	-3.65220	0.0002600** *
D_{PC}	12.34489	1.17463	10.5096	< 2. 2E-16***

T_{PM} = intervessel pit membrane thickness; P_{FWFA} = proportion of fiber wall area per fiber cell area; T_V = vessel wall thickness; D_{PC} = pit chamber depth; *** *p*-value < 0.001; ** *p*-value < 0.01; * *p*-value < 0.05

Table S5 The best multiple regression model, based on AIC scores, of anatomical features, explaining P_{88} variation in stems of the four *Arabidopsis thaliana* accessions studied.

Predictors	Estimate	Std. Error	z value	Pr (> z)
(Intercept)	4.16481	0.67485	6.17150	6.764E-10***
T_{PM}	11.37418	3.08554	3.68630	0.0002276***
(T_{VW}/D_{MAX})²	-42.08524	16.36473	-2.57170	0.0101199*
P_{FWFA}	-1.24828	0.62798	-1.98780	0.0468351*
V_G	-0.77311	0.46031	-1.67950	0.0930509
D_{PC}	-15.82159	1.66181	-9.52070	< 2.2E-16***

T_{PM} = intervessel pit membrane thickness; (T_{VW}/D_{MAX})² = theoretical vessel implosion resistance; P_{FWFA} = proportion of fiber wall area per fiber cell area; V_G = vessel grouping index; D_{PC} = pit chamber depth; *** *p*-value < 0.001; ** *p*-value < 0.01; * *p*-value < 0.05

Chapter 2: Intervessel pit membrane thickness and embolism resistance

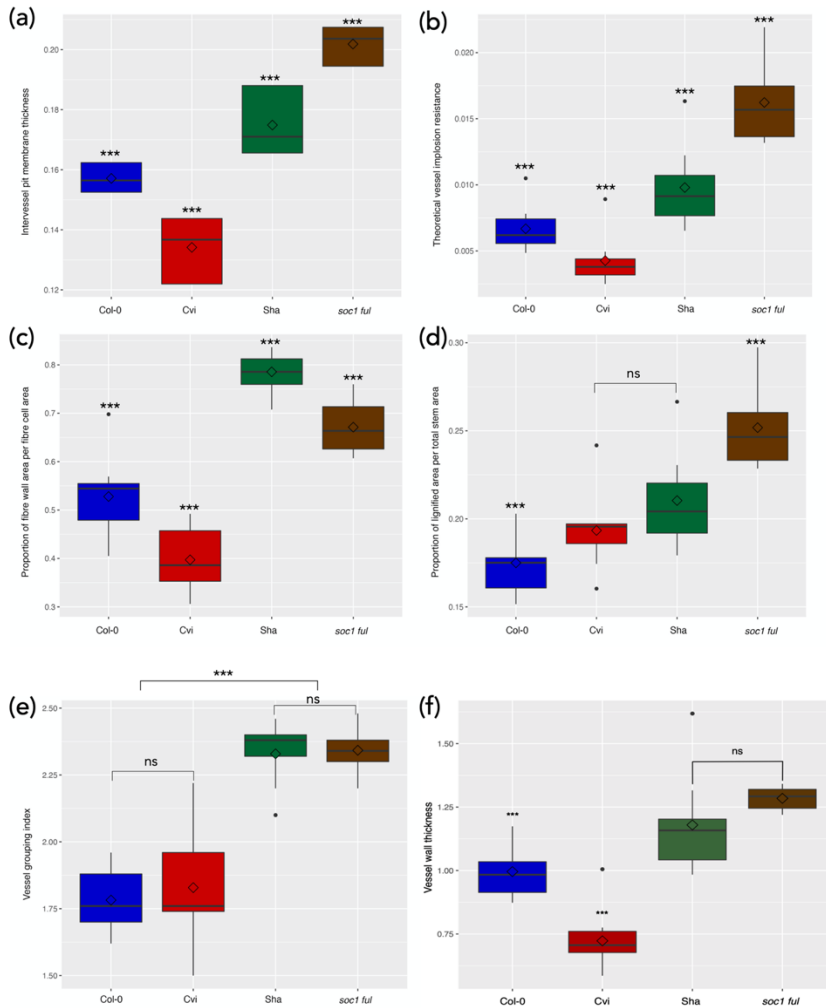


Figure S1 Boxplots showing anatomical variation within and between accessions. (a) boxplot of intervessel pit membrane thickness (T_{PM}); (b) boxplot of theoretical vessel implosion resistance (T_{VW}/D_{MAX}^2); (c) boxplot of proportion of fiber wall area per fiber cell area (PF_{WFA}); (d) boxplot of proportion of lignified area per total stem area (P_{LIG}); (e) boxplot of vessel grouping index (V_G); ns = p -value > 0.05; *** p -value < 0.01

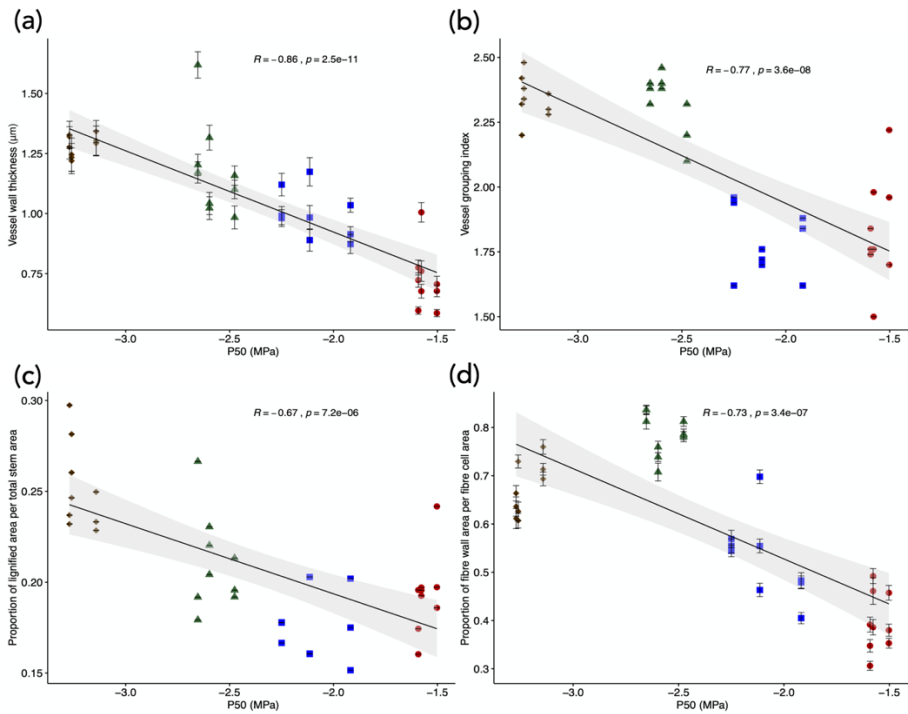


Figure S2 Scatter plots with regression lines showing the relationships between anatomical characters and P_{50} . (a) the negative correlation between vessel grouping index (V_G) and P_{50} ; (b) negative correlation between proportion of fiber wall area per fiber cell area (PF_{WF_A}) and P_{50} ; (c) negative correlation between proportion of lignified area per total stem area (P_{LIG}) and P_{50} . Colours and styles refer to the accession studied: Col-0 (blue-filled square), Cvi (red-filled circle), Sha (green-filled triangle) and *soc1ful* (brown-filled diamond).

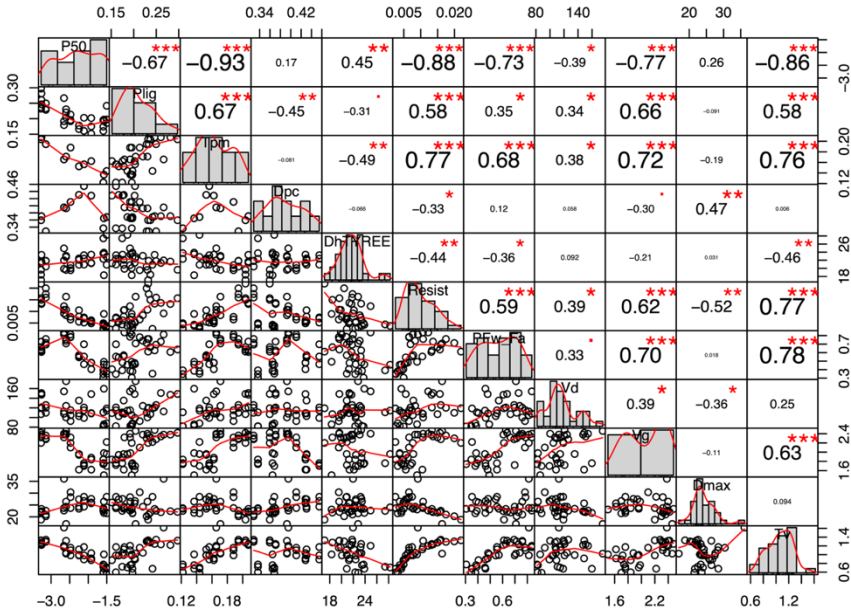


Figure S3 The pairwise scatter plots based on Pearson’s correlation analysis showing the correlations of P_{50} (response variable) and each stem anatomical trait studied (predictive variables) and between all the predictive variables comprising proportion of lignified area per total stem area (P_{LIG}), intervessel pit membrane thickness (T_{PM}), pit chamber depth (D_{PC}), hydraulically weighted vessel diameter (D_H or D_{HTYREE}), theoretical vessel implosion resistance ($(T_{VW}/D_{MAX})^2$ or Resist), proportion of fiber wall area per fiber cell area (P_{FWFA}), vessel density (V_D), vessel grouping index (V_G), maximum vessel lumen diameter (D_{MAX}), and vessel wall thickness (T_V) *** p -value < 0.01; ** p -value < 0.01; * p -value < 0.05.

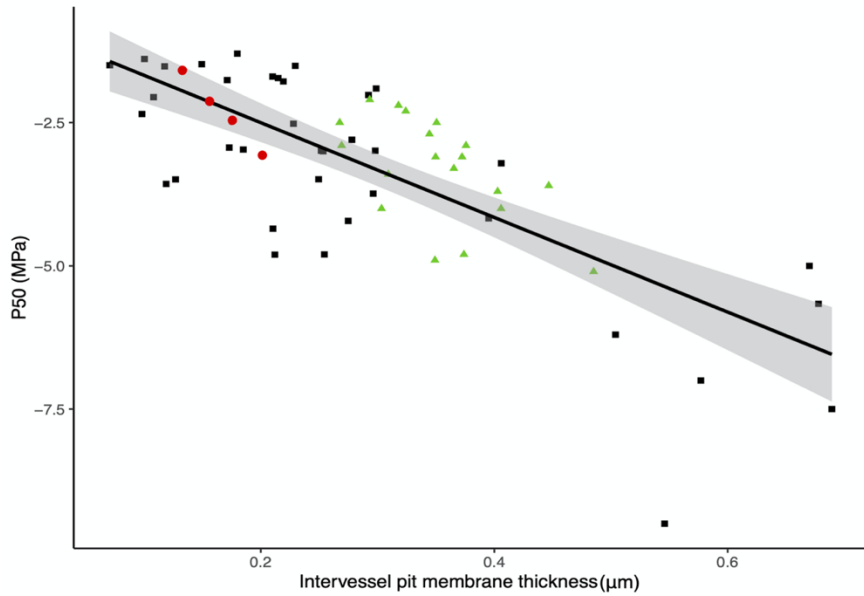


Figure S4 Scatter plot with regression line showing the relationship between P_{50} and intervessel pit membrane thickness (T_{PM}) of published woody and herbaceous angiosperms from Li *et al.* (2016; woody species marked as black-filled squares), Dória *et al.* (2018, 2019; mostly herbaceous species marked as green-filled triangles), and this study (red-filled circles).

Chapter 2: Intervessel pit membrane thickness and embolism resistance

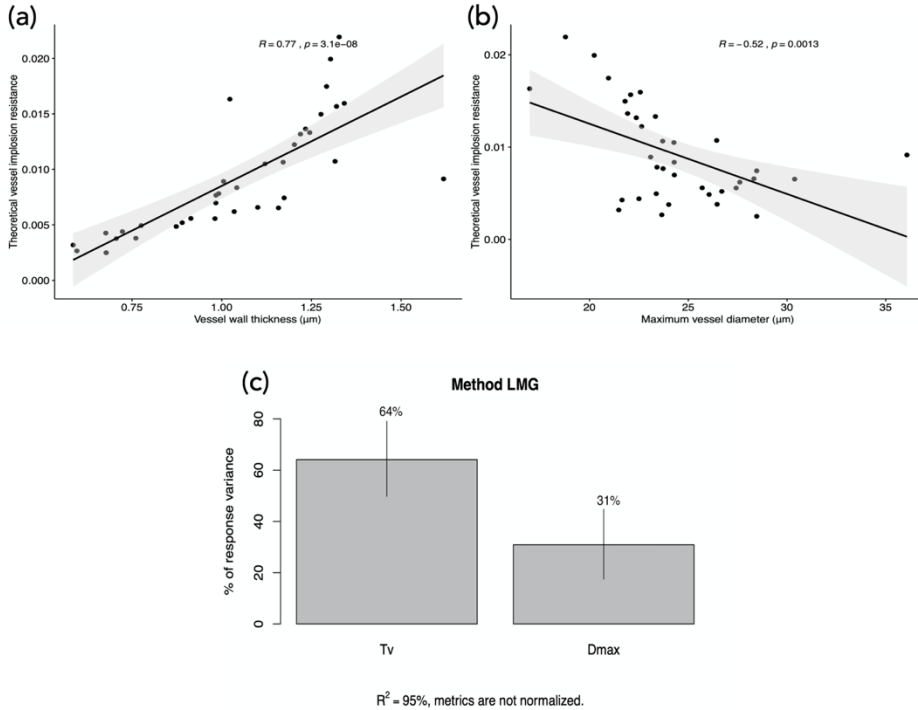


Figure S5 Scatter plots with regression lines showing the relationship between (a) theoretical vessel implosion resistance ($(T_{VW}/D_{MAX})^2$) and vessel wall thickness (T_V), and (b) theoretical vessel implosion resistance ($(T_{VW}/D_{MAX})^2$) and maximum vessel lumen diameter (D_{MAX}); (c) the relative importance of theoretical vessel implosion resistance variation is mainly explained by vessel wall thickness (T_V) based on R^2 contribution averaged over orderings among regressors.

